J Polym Res (2016) 23: 34
DOI 10.1007/s10965-016-0930-8

ORIGINAL PAPER

Influence of preparation conditions on structural and dielectric properties of PVDF–MoS_2 nanotubes composite films

Ana Varlec[1] · **Andreja Eršte**[1] · **Vid Bobnar**[1] · **Maja Remškar**[1]

Received: 11 August 2015 / Accepted: 24 January 2016 / Published online: 28 January 2016

Abstract Poly(vinylidene fluoride) composite films with MoS_2 nanotubes were prepared from solutions using the doctor blade method and dried under various temperatures. While FTIR-ATR and Raman spectroscopy have revealed that composite films dried at room temperature are homogeneous and crystallize mainly in the γ-phase, a decrease in porosity upon addition of MoS_2 has been observed using scanning electron microscopy. Dielectric investigations revealed (i) a decrease from $\varepsilon' \sim 7$ in pure polymer to $\varepsilon' \sim 4$ in composite with 1 wt% of MoS_2, and (ii) a slight increase in ε' and σ' values upon further addition of MoS_2. Films dried at 110 °C were heterogeneous and FTIR-ATR has shown an increase in α-phase content upon addition of 1 wt% of MoS_2. In this case, high values of $\varepsilon' \sim 10$ that increased slightly upon increasing amount of MoS_2 in the film have been measured. By showing a direct relation between structure and dielectric response, it is suggested that the dielectric properties of poly(vinylidene fluoride)–MoS_2 nanotubes composites can be tailored by changing the preparation conditions.

Keywords PVDF · MoS_2 nanotubes · Composites · Dielectric response · Raman spectroscopy · FTIR-ATR

✉ Ana Varlec
ana.varlec@ijs.si

[1] Condensed Matter Physics Department, Jožef Stefan Institute, Jamova cesta 39, 1000 Ljubljana, SI, Slovenia

Introduction

Poly(vinylidene fluoride) (PVDF) is a semicrystalline polymer, which has been attracting considerable attention due to its ferroelectric, piezoelectric, and pyroelectric properties, high elasticity and high dielectric constant values [1–3]. Its diverse morphology, obtained through easily controlled processing conditions, make it compelling for use in a vast array of applications in the areas of biomedicine, energy generation and storage, filtration, sensors and actuators [1, 3–6]. In PVDF, the molecular formula of which is $(CH_2 - CF_2)_n$, the dipole moment attached to the main chain can adopt various orientations depending on the conformation of the chain. The variety of ways in which the chains can pack into crystalline structures results in several polymorphous modifications, i.e., the diversity of PVDF arises partly due to its polymorphism, enabling crystallization into at least five phases (commonly known as the α, β, γ, δ and ε- phases) [1, 4, 7–9]. The non-polar α-phase is the most common, and is usually obtained by melt crystallization at temperatures below 160 °C. At higher temperatures a co-existence of the non-polar α and polar γ-phase occurs (the γ-phase occurrence increases with crystallization temperature and time) [1, 3, 8]. The most polar PVDF phase, the β-phase, can be obtained either from α-phase films by mechanical deformation or electrical poling [1, 3] or from the melt using high pressures [10] or epitaxial techniques [11]. Nonetheless, these methods often induce undesirable structural deformations or microstructural limitations which may hinder specific applications as electro-optical sensors and non-volatile memories [12, 13], for example. Concomitantly, alternative methods have been developed, i.e., the β-phase of PVDF has been obtained by doping the polymer with fillers such as $BaTiO_3$ [14], clays [15, 16], hydrated ionic salts [17], TiO_2 [18], ferrite nanoparticles [18] or multi-walled carbon nanotubes [19].

Molybdenum disulfide nanotubes (MoS_2 NTs) are widely known for their use as a lubricant [20] and recent studies have shown that they are also potentially useful use in other applications, such as hydrogen storage [21–23], catalysis [24], and sensor technologies [25]. Co-axial MoS_2 NTs with split walls have an exfoliated structure and have possible applications in polymer composites such as self-lubricating and anti-corrosive coatings or in solar cell applications [9]. Although the structural and dielectric properties of various systems composed of nanofillers within a polymer matrix were studied and characterized extensively over the last decade [3, 19, 26, 27], very little research and development has been performed on polymer nanocomposites using MoS_2 NTs as nanofillers [9]. In order to further develop our knowledge of polymer composites with MoS_2 NTs, we have investigated the influence of preparation conditions on the structural and dielectric properties of PVDF-MoS_2 NTs composite films using Fourier transform infrared spectroscopy (FTIR), Raman spectroscopy, and high-resolution dielectric spectroscopy across broad frequency and temperature ranges.

Materials and methods

PVDF-MoS_2 nanotubes (NTs) composite films were prepared from 20 wt% solutions of PVDF (301-F grade, Arkema) in dimethylformamide (DMF, Sigma Aldrich, ≥ 99 %) and 0 wt% (pure PVDF), 1 wt%, and 2 wt% MoS_2 nanotubes (Nanotul Ltd. Ljubljana, Slovenia) with respect to the PVDF [9]. The solutions were air-cast on a glass plate and drawn by doctor blade (thickness of 300 μm) on a film applicator (Erichsen). Films were then dried for 24 h at 50 % relative humidity at 22 °C and removed from the glass plate after the drying process was completed. A second set of films was dried at 110 °C. In the remaining text, the samples dried at 22 °C or 110 °C will be referred to as the room temperature (RT) or high temperature (HT) samples, respectively. The thickness of the films was 60 μm to 75 μm (RT samples) and 21 μm to 24 μm (HT samples). Their morphology was studied with field emission scanning electron microscope (SEM), Supra 36 VP, Carl Zeiss.

Table 1 Distinctive vibrational modes for different PVDF conformations in cm^{-1} units [28–31]

IR active			Raman active		
α	β	γ	α	β	γ
764		776			
796		812	795		812 w
855	840	833, 838		839 vs	839 s
976	884	883			
1149	1179	1117			
1210 1383	1279	1234			

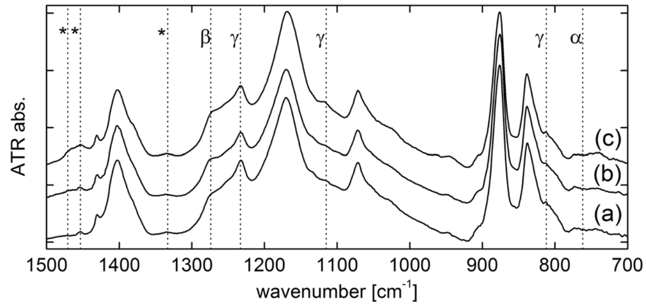

Fig. 1 FTIR-ATR spectra of RT PVDF (**a**), RT PVDF–1 wt% MoS_2 (**b**) and RT PVDF–2 wt% MoS_2 (**c**) films. All spectra are very similar and only γ-phase distinctive band at 1234 cm^{-1} can be observed

Fourier-transform infrared spectra (FTIR) in the mid-infrared region were measured by Perkin Elmer Spectrum 400 equipped with a Pikes GladiATR accessory and were recorded with 2 cm^{-1} resolution. For comparison, all spectra were normalized to a unit area since the porosity of the films, and consequently the overall intensity of the FTIR-ATR signal, was influenced by the addition of MoS_2 NTs.

Raman spectra were recorded with confocal Raman imaging system alpha300R (WITec) with a frequency doubled Nd:YAG laser (532 nm) in backscattering geometry. A full laser power of approximately 40 mW was used for the non-sensitive films (pure PVDF) and a reduced power of 6 mW was used for the sensitive samples (composites). A spectrometer with a grating of 1800 lines/mm was used. The acquisition time for a single spectrum was 5 to 10 min. In order to get sufficient sampling,

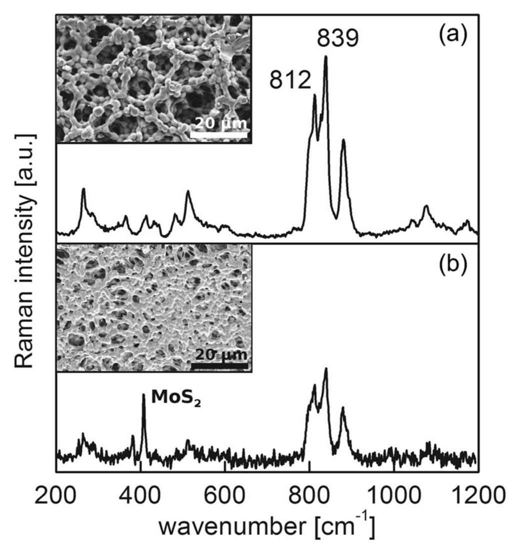

Fig. 2 Raman spectra of RT pure PVDF (**a**) and RT PVDF–1 wt% MoS_2 films (**b**). The γ-phase distinctive band at 812 cm^{-1} is clearly visible. Spectrum (**b**) is very similar to spectrum (**a**), with addition of 382 cm^{-1} and 408 cm^{-1} MoS_2 bands. Insets show SEM images of corresponding films' top surface. Porosity of RT PVDF–1 wt% MoS_2 film is decreased compared to pure PVDF RT film

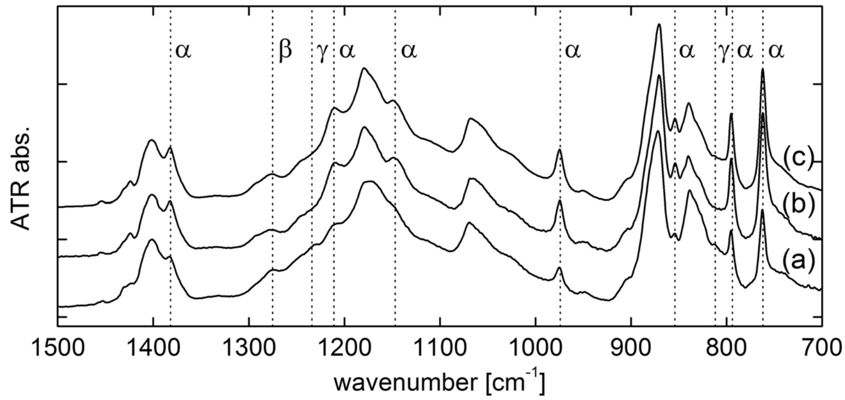

Fig. 3 FTIR-ATR spectra of HT PVDF (**a**), HT PVDF–1 wt% MoS_2 (**b**) and HT PVDF–2 wt% MoS_2 (**c**) films at their *top side*

several single point spectra measurements on each sample were performed.

For dielectric measurements, films were covered with sputtered electrodes (100 nm of gold on 10 nm of chromium for better adhesion). The complex dielectric constant $\varepsilon^*(\Omega, T) = \varepsilon' - i\varepsilon''$ was measured with an HP4284A Precision LCR Meter using the amplitude of the probing AC electric signal of 1 V. The real part of the complex ac conductivity $\sigma^* = \sigma' + i\sigma''$ was calculated via $\sigma' = 2\pi\nu\varepsilon'\varepsilon''$, with ε' being the permittivity of free space. After heating the samples to 350 K, the dielectric response was detected during cooling runs at a rate of 0.9 Kmin^{-1}. The temperature of the samples was stabilized within ±0.01 K by using a lock-in bridge technique with a platinum resistor Pt100 as a thermometer.

Results and discussion

Vibrational spectroscopy

Numerous reports in the literature distinguish different PVDF phases on the basis of characteristic vibrational modes [28–31]. Vibrational spectroscopy gives direct information on the conformation of the chains, however, it does not provide information on the packing of the chains into crystals, which becomes relevant in the case of δ- and α-phase, which have the same conformations but different crystalline structures [32]. Nonetheless, the standard nomenclature for conformations is used in this work, i.e. α-phase is used to denote the TGTG' conformation, β for TTTT and γ for TTTGTTTG'. Both infrared (IR) active and Raman active modes distinctive for these phases are summarized in Table 1. The α-phase has many distinctive bands in the mid-IR (764 cm^{-1}, 796 cm^{-1}, 976 cm^{-1}) and in Raman spectra (795 cm^{-1}). The γ-phase has one distinctive Raman active band (812 cm^{-1}) and β-phase has one distinctive IR active band (1279 cm^{-1}). Therefore, only with a combination of both vibrational techniques can we clearly distinguish the β- and γ-phases.

There is another advantage to using both techniques: the probed area using FTIR-ATR is 1 mm^2 whereas the probed area for confocal Raman spectroscopy is less than 1 μm^2. FTIR-ATR thus provides averaged information over larger scales, while Raman spectroscopy provides local information and is suitable for checking homogeneity of the samples.

FTIR-ATR spectra of RT PVDF–MoS_2 films are presented in Fig. 1. Since MoS_2 has no characteristic bands in the mid-IR part [33] the absorption is related to PVDF only. The pure PVDF (a) and composites with MoS_2 added in the range of 1–2 wt% (b,c) all have very similar spectra. The γ-phase distinctive band at 1234 cm^{-1} is clearly observed, while the β-phase distinctive band at 1279 cm^{-1} appears as a shoulder. There is no α-phase distinctive band, and we can thus conclude that (i)

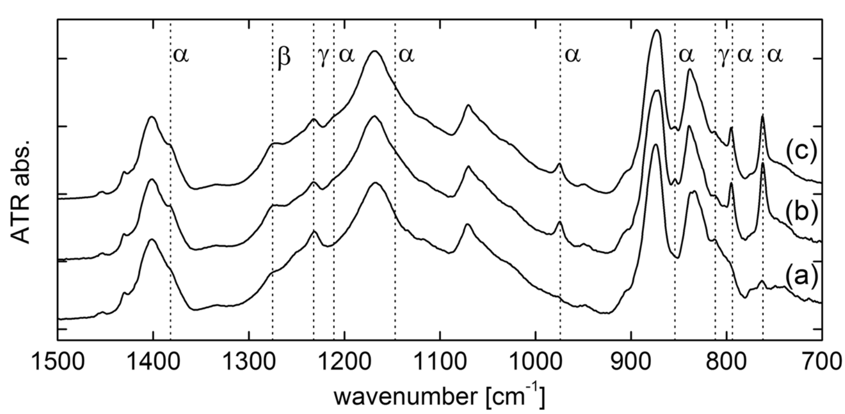

Fig. 4 FTIR-ATR spectra of HT PVDF (**a**), HT PVDF–1 wt% MoS_2 (**b**) and HT PVDF–2 wt% MoS_2 (**c**) films at their *bottom side*

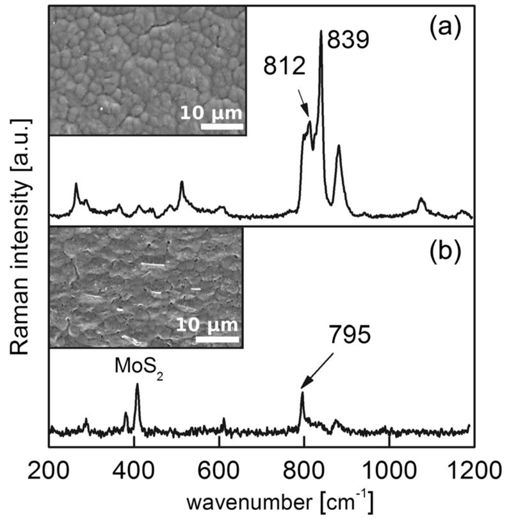

Fig. 5 Raman spectrum of HT pure PVDF film in β-phase rich point (**a**) with inset showing SEM of top surface of the film. Raman spectrum of PVDF–1 wt% MoS_2 (**b**) is dominated by α-phase. In the SEM image (inset) we can see MoS_2 NTs inside films

films prepared at room temperature mainly obtain the γ-phase conformation and (ii) the addition of MoS_2 NTs does not influence the conformation of PVDF chains. Although the peaks, marked with an asterisk in Fig. 1, cannot be explained by any of the possible conformations or crystalline structures of PVDF, the 1454 cm^{-1} band, which is especially evident in the case of pure PVDF and less evident 1330 cm^{-1} band can be attributed to irregular head-to-head and tail-to-tail linkages [31].

The Raman spectra of RT pure PVDF film (Fig. 2a) are in accordance with the γ-phase in the majority of randomly selected points on the sample. There is no trace of α-phase bands, however the presence of β-phase cannot be excluded solely on the basis of the Raman spectra data, as explained above. Typical single point spectra of RT PVDF–1 wt% MoS_2 (Fig. 2b) and PVDF–2 wt% MoS_2 films are very similar to the spectrum of RT pure PVDF. This is in agreement with the FTIR-ATR data which show that MoS_2 NTs do not change the phase of RT PVDF films (see Fig. 1). The Raman spectra of RT PVDF–MoS_2 films reveal intense 382 cm^{-1} and 408 cm^{-1} bands that belong to MoS_2 [33]. We also observe that PVDF–MoS_2 composite films are less stable upon laser illumination in comparison to pure films. Under high power illumination, spectra are either transformed or decomposition of the sample takes place. This sensitivity can be explained by the high light absorption coefficient of MoS_2 [34] and consequent heating of the polymer in the vicinity of NTs.

SEM micrographs of top surfaces of RT films are shown in the insets to Fig. 2. The RT pure PVDF film is porous, which is typical when drop casting PVDF solution at low temperature [8]. Porosity is greatly reduced with the addition of MoS_2 NTs.

Although the ATR spectra of HT PVDF–MoS_2 on the top (Fig. 3) and bottom (Fig. 4) surface vary slightly, it can be seen that MoS_2 NTs influence the crystallization of films dried at 110 °C. Upon addition of MoS_2 NTs the α-phase bands become more noticeable.

While the top surface spectra reveal a very weak β-phase band and practically no γ-phase band, the bottom surface has a less uniform structure in which all spectra have notable β and γ contributions. In both cases intensity of the α bands is increased upon addition of MoS_2 NTs. There is no notable difference between the spectra of PVDF–2 wt% MoS_2 NTs film and the spectra of PVDF–1 wt% MoS_2.

The Raman spectra of HT pure PVDF sample at different random points vary between phases, e.g., some points are rich in β and γ-phase (Fig. 5a), while other are rich in α-phase. In HT PVDF–MoS_2 films, spectra in the majority of points show α-phase (Fig. 5b). These results are consistent with FTIR-ATR results.

Fig. 6 The real, ε', and the imaginary, ε", parts of the complex dielectric constant and the real, σ', part of the complex ac conductivity vs. temperature, obtained at various frequencies in RT pure PVDF and PVDF–MoS_2 films

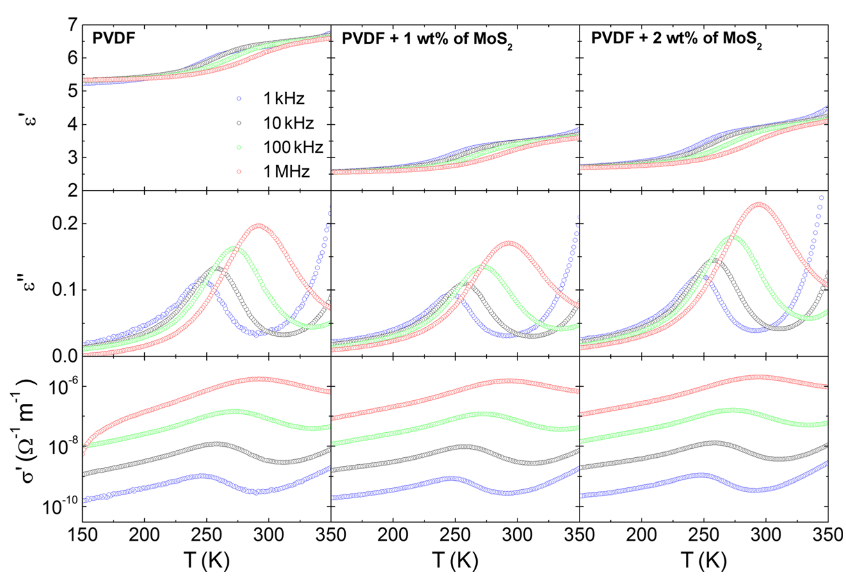

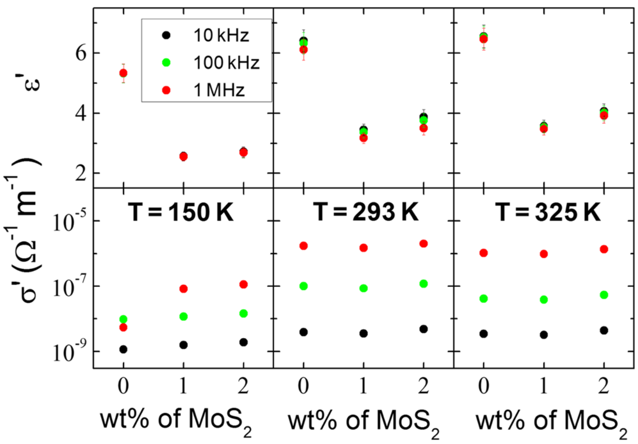

Fig. 7 ε' and σ' vs. wt% of MoS_2, detected at 150 K, 293 K, and 325 K in RT PVDF–MoS_2 films

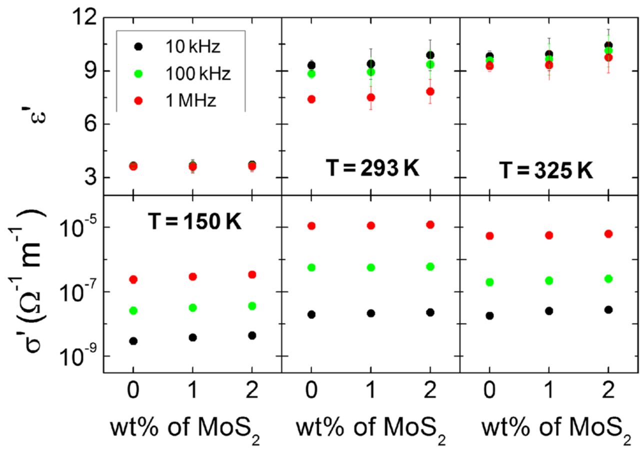

Fig. 9 ε' and σ' vs. wt% of MoS_2 nanotubes, detected at 150 K, 293 K, and 325 K in PVDF–MoS_2 films, prepared at 393 K

The morphology of the HT pure PVDF and HT PVDF–1 wt% MoS_2 films are shown in the insets to Figs. 5a and 5b, respectively. The spherulites are completely interconnected and the surface is clearly not porous. The addition of MoS_2 nanotubes does not change the morphology.

Dielectric response

Dielectric spectroscopy is a powerful tool for the research and development of novel dielectric materials (e.g. PVDF-based polymers [35]) as it enables us to understand the behavior of interfaces at the boundary of two different materials or material phases and accurately control material properties.

Figure 6 shows a comparison of the temperature-dependent dielectric response of RT pure PVDF and PVDF–MoS_2 films. The dielectric relaxation, which can clearly be seen in the temperature interval of 200 K to 300 K is known to be a dynamic manifestation of the glass-to-rubber transition that takes place in the amorphous part of PVDF [36, 37]. The addition of 1 wt% of MoS_2 nanotubes strongly decreases the values of the real part of the complex dielectric constant, ε', while the values of the imaginary part, ε" (which represent the dielectric losses, i.e., the electrical conductivity of the system), remain almost unchanged, and the characteristic dynamic peaks in ε"(T) occur at the same temperatures in all samples. Such a strong change in ε' values unaccompanied by notable changes in dielectric losses indicates that the addition of MoS_2 nanotubes either predominantly induces changes in the order of the PVDF structure or decreases the porosity of PVDF and at the same time does not implement any additional defects into the material structure itself. The latter was observed in SEM (see inset to Fig. 2) which revealed that the addition of MoS_2 NTs notably decreased the porosity of the film while vibrational spectroscopy showed no significant changes to the structure of PVDF.

On further addition of the nanotubes, the values of both ε' and ε" slightly increase, which can be attributed to the increased electrical conductivity of the composite due to the

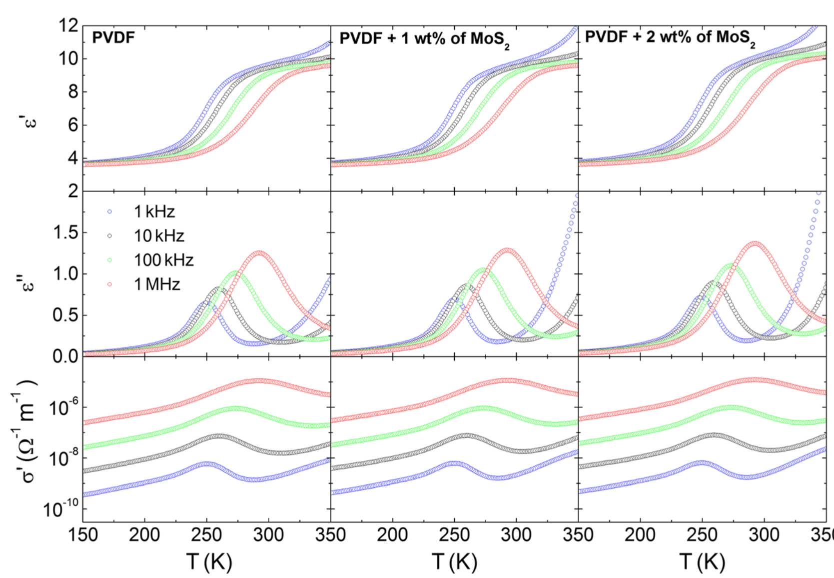

Fig. 8 ε', ε", and σ' vs. temperature, obtained at various frequencies in HT PVDF–MoS_2 films

semiconducting [23] MoS_2 inclusions (as σ' and ε" are directly related and influence ε' via Kramers-Kronig relations). This effect becomes even more evident in Fig. 7, which depicts the values of the real parts of the complex dielectric constant and ac electrical conductivity, detected in all three samples at 150 K, 293 K and 325 K.

Figure 8 shows the temperature-dependent dielectric response of HT PVDF–MoS_2 films. In this case the pure PVDF film reveals different dielectric behavior than the RT PVDF film (see Fig. 9), which can be attributed to the rich morphology of the PVDF itself [1, 38]. Both Raman spectroscopy and FTIR-ATR have confirmed the presence of α-, β- and γ-phases (see Figs. 3, 4 and 5). It is evident from Fig. 9 that upon addition of 1 wt% of MoS_2 NTs there is no notable increase or decrease in the values of ε', ε", and σ', which can be attributed to the superposition of two opposite effects. First, the presence of semiconducting MoS_2 NTs increases the values of ε', ε", and σ' due to the Kramers-Kronig relations. Second, the increase of the non-polar α-phase content causes a decrease to the ε', ε", and σ' [1, 8, 28]. Upon increasing to 2 wt% of MoS_2 NTs, the values of all, ε', ε", and σ' only slightly increase, which can be attributed mostly to the addition of semiconducting MoS_2 nanotubes, since the α-phase content, detected by vibrational spectroscopy, has no significant increase.

Conclusions

Poly(vinylidene fluoride) [PVDF] composite films with 0, 1, and 2 wt% of MoS_2 nanotubes were prepared from solutions using the doctor blade method and dried at either room temperature or 110 °C. Vibrational spectroscopy has shown that films dried at room temperature are homogeneous and crystallize mainly in the γ-phase, regardless of the MoS_2 concentration. Dielectric spectroscopy results revealed a strong decrease in the value of the dielectric constant from ε' ~ 7 (pure PVDF) to ε' ~ 4 (PVDF with 1 wt% of MoS_2), which may be attributed to a decrease of porosity that was observed with SEM.

PVDF–MoS_2 films dried at 110 °C were heterogeneous and the α-phase content increased upon addition of 1 wt% MoS_2 nanotubes. Detailed analysis of FTIR-ATR and Raman spectroscopy results has shown that these films in fact consist of small areas containing individual α, β, or γ-phase and the top surface is richer in α-phase in comparison to the bottom surface of the film. In this case, high values of ε' ~ 10 have been detected in the pure PVDF film. Upon addition of 1 wt% MoS_2 no notable change in ε', ε", and σ' values was detected and it may be assumed that this is a direct consequence of the superposition of two opposite effects: (i) the presence of semiconducting MoS_2 nanotubes, which increases the values of the dielectric constant, and (ii) the increasing content of the non-polar α-phase in the PVDF, which decreases dielectric constant values. Upon further addition of MoS_2 a slight increase of in ε', ε", and σ' values was detected, which can be attributed mostly to the addition of semiconducting MoS_2 nanotubes, since the α-phase content remained the same.

To summarize, we have shown that the dielectric response of PVDF–MoS_2 nanotubes composite films is a direct consequence of structural properties, revealed by FTIR-ATR, Raman spectroscopy, and SEM. It can thus be suggested that the dielectric properties of PVDF–MoS_2 nanotubes composites can be tailored by changing their preparation conditions.

Acknowledgments This project was financially supported by Slovenian Research Agency under project 1000-11-310181 and programs P1-0099 and P1-0125 and by Ministry of Education, Science and Sport of Republic of Slovenia and European Social Fund under project PR-05648.

Compliance with ethical standards

Conflict of interest There is no conflict of interest.

References

1. Lovinger AJ (1983) Ferroelectric polymers. Science 220:1115–1121
2. Lovinger AJ (1982) Annealing of poly (vinylidene fluoride) and formation of a fifth phase. Macromolecules 15:40–44
3. Martins P, Lopes AC, Lanceros-Mendez S (2014) Electroactive phases of poly(vinylidene fluoride): determination, processing and applications. Prog Polym Sci 39:683–706. doi:10.1016/j.progpolymsci.2013.07.006
4. Lovinger AJ (1981) Conformational defects and associated molecular motions in crystalline poly(vinylidene fluoride). J Appl Phys 52:5934. doi:10.1063/1.328522
5. Nix EL, Ward IM (1986) The measurement of the shear piezoelectric coefficients of polyvinylidene fluoride. Ferroelectrics 67:137–141. doi:10.1080/00150198608245016
6. Zhang QM, Bharti V, Kavarnos G (2002) Poly(vinylidene fluoride) (PVDF) and its copolymers. Encycl. Smart Mater
7. Hilczer B, Szafrański M, Hilczer A (2012) Pressure-induced changes in the dielectric response of polymer relaxors. Appl Phys Lett 100:052904. doi:10.1063/1.3681372
8. Gregorio Jr R, Ueno EM (1999) Effect of crystalline phase, orientation and temperature on the dielectric properties of poly (vinylidene fluoride)(PVDF). J Mater Sci 34:4489–4500
9. Remškar M, Iskra I, Jelenc J, et al. (2013) A novel structure of polyvinylidene fluoride (PVDF) stabilized by MoS_2 nanotubes. Soft Matter 9:8647. doi:10.1039/c3sm51279g
10. Scheinbeim J, Nakafuku C, Newman BA, Pae KD (1979) High-pressure crystallization of poly(vinylidene fluoride). J Appl Phys 50:4399. doi:10.1063/1.326429
11. Lovinger A (1982) Poly(vinylidene fluoride). In: DC B (ed) Dev. Cryst. Polym. Springer, Netherlands, pp. 195–273
12. Dahiya RS, Cattin D, Adami A, et al. (2011) Towards tactile sensing system on chip for robotic applications. IEEE Sensors J 11:3216–3226. doi:10.1109/JSEN.2011.2159835

13. Henkel K, Lazareva I, Mandal D, et al. (2009) Electrical investigations on metal/ferroelectric/insulator/semiconductor structures using poly[vinylidene fluoride trifluoroethylene] as ferroelectric layer for organic nonvolatile memory applications. J Vac Sci Technol B 27:504–507. doi:10.1116/1.3043476
14. Ye H-J, Shao W-Z, Zhen L (2013) Crystallization kinetics and phase transformation of poly(vinylidene fluoride) films incorporated with functionalized $BaTiO_3$ nanoparticles. J Appl Polym Sci 129:2940–2949. doi:10.1002/app.38949
15. Priya L, Jog JP (2002) Poly(vinylidene fluoride)/clay nanocomposites prepared by melt intercalation: crystallization and dynamic mechanical behavior studies. J Polym Sci B Polym Phys 40:1682–1689. doi:10.1002/polb.10223
16. Lopes AC, Costa CM, Tavares CJ, et al. (2011) Nucleation of the electroactive γ phase and enhancement of the optical transparency in low filler content poly(vinylidene)/clay nanocomposites. J Phys Chem C 115:18076–18082. doi:10.1021/jp204513w
17. Benz M, Euler WB, Gregory OJ (2002) The role of solution phase water on the deposition of thin films of poly(vinylidene fluoride). Macromolecules 35:2682–2688. doi:10.1021/ma011744f
18. Martins P, Moya X, Phillips LC, et al. (2011) Linear anhysteretic direct magnetoelectric effect in $Ni_{0.5}Zn_{0.5}Fe_2O_4$ /poly(vinylidene fluoride-trifluoroethylene) 0–3 nanocomposites. J Phys Appl Phys 44:482001. doi:10.1088/0022-3727/44/48/482001
19. Dang Z-M, Wang L, Yin Y, et al. (2007) Giant dielectric permittivities in functionalized carbon-nanotube/electroactive-polymer nanocomposites. Adv Mater 19:852–857. doi:10.1002/adma.200600703
20. Clauss FJ (1972) Chapter 4 - molybdenum disulfide. In: Clauss FJ (ed) Solid lubr. Self-Lubr. Solids. Academic Press, pp. 75–112
21. Chen J, Kuriyama N, Yuan H, et al. (2001) Electrochemical hydrogen storage in MoS_2 nanotubes. J Am Chem Soc 123:11813–11814. doi:10.1021/ja017121z
22. Wang J, Han S, Zhang W, et al. (2013) Effects of MoS2 addition on the hydrogen storage properties of $2LiBH_4$–MgH_2 systems. Int J Hydrog Energy 38:14631–14637. doi:10.1016/j.ijhydene.2013.08.129
23. Zhao Y, Zhang Y, Yang Z, et al. (2013) Synthesis of MoS_2 and MoO_2 for their applications in H_2 generation and lithium ion batteries: a review. Sci Technol Adv Mater 14:043501. doi:10.1088/1468-6996/14/4/043501
24. Cesano F, Bertarione S, Piovano A, et al. (2011) Model oxide supported MoS_2 HDS catalysts: structure and surface properties. Catal Sci Technol 1:123. doi:10.1039/c0cy00050g
25. Loan P. T. K., Zhang W, Lin C.-T., et al. (2014) Graphene/MoS_2 Heterostructures for Ultrasensitive Detection of DNA Hybridisation. Advanced Materials 26:4838–4844. doi:10.1002/adma.201401084
26. Wang L, Dang Z-M (2005) Carbon nanotube composites with high dielectric constant at low percolation threshold. Appl Phys Lett 87:042903. doi:10.1063/1.1996842
27. Yu L, Cebe P (2009) Effect of nanoclay on relaxation of poly(vinylidene fluoride) nanocomposites. J Polym Sci B Polym Phys 47:2520–2532. doi:10.1002/polb.21864
28. Połomska M, Hilczer B, Markiewicz E, et al. (2010) Effect of processing conditions on the dielectric and Raman response of electroactive polymers. Ferroelectrics 405:138–145. doi:10.1080/00150193.2010.483192
29. Tashiro K, Kobayashi M, Tadokoro H (1981) Vibrational spectra and disorder-order transition of poly (vinylidene fluoride) form III. Macromolecules 14:1757–1764
30. Boccaccio T, Bottino A, Capannelli G, Piaggio P (2002) Characterization of PVDF membranes by vibrational spectroscopy. J Membr Sci 210:315–329
31. Nalwa HS (1995) Ferroelectric polymers: chemistry, physics, and applications. Marcel Dekker, Inc., New York
32. Bachmann M, Gordon WL, Weinhold S, Lando JB (1980) The crystal structure of phase IV of poly(vinylidene fluoride). J Appl Phys 51:5095. doi:10.1063/1.327425
33. Wieting TJ, Verble JL (1971) Infrared and Raman studies of long-wavelength optical phonons in hexagonal MoS_2. Phys Rev B 3:4286
34. Jaegermann W (1992) Surface studies of layered materials in relation to energy converting interfaces. In: Aruchamy A (ed) Photoelectrochem. Photovolt. Layer. Semicond. Kluwer Academic Publishers, Dordrecht, pp. 195–295
35. Bobnar V, Vodopivec B, Levstik A, et al. (2003) Dielectric properties of relaxor-like vinylidene fluoride − trifluoroethylene-based electroactive polymers. Macromolecules 36:4436–4442. doi:10.1021/ma034149h
36. Furukawa T (1989) Ferroelectric properties of vinylidene fluoride copolymers. Phase Transit 18:143–211. doi:10.1080/01411598908206863
37. Bharti V, Xu HS, Shanthi G, et al. (2000) Polarization and structural properties of high-energy electron irradiated poly(vinylidene fluoride-trifluoroethylene) copolymer films. J Appl Phys 87:452. doi:10.1063/1.371883
38. Hilczer B, Smogór H, Goslar J (2006) Dielectric response of polymer relaxors. J Mater Sci 41:117–127. doi:10.1007/s10853-005-5949-x